Highly featured amorphous silicon nanorod arrays for high-performance lithium-ion batteries

Samaneh Soleimani-Amiri, Seied Ali Safiabadi Tali, Soheil Azimi, Zeinab Sanaee, and Shamsoddin Mohajerzadeh[a)]
Thin Film and Nanoelectronics Lab, Nanoelectronics Center of Excellence, School of Electrical and Computer Engineering, University of Tehran, Tehran 143957131, Iran

(Received 22 September 2014; accepted 4 November 2014; published online 14 November 2014)

High aspect-ratio vertical structures of amorphous silicon have been realized using hydrogen-assisted low-density plasma reactive ion etching. Amorphous silicon layers with the thicknesses ranging from 0.5 to 10 μm were deposited using radio frequency plasma enhanced chemical vapor deposition technique. Standard photolithography and nanosphere colloidal lithography were employed to realize ultra-small features of the amorphous silicon. The performance of the patterned amorphous silicon structures as a lithium-ion battery electrode was investigated using galvanostatic charge-discharge tests. The patterned structures showed a superior Li-ion battery performance compared to planar amorphous silicon. Such structures are suitable for high current Li-ion battery applications such as electric vehicles. © *2014 AIP Publishing LLC*. [http://dx.doi.org/10.1063/1.4902068]

Hydrogenated amorphous silicon (a-Si:H) has important applications in thin film transistors (TFTs), solar cells, lithium-ion batteries, and RF-ID tags.[1–4] Owing to its low temperature processing and also its compatibility with glass substrates, amorphous silicon is a highly favorable material for large area electronic and photonic applications.[5] The use of amorphous silicon in large area X-ray imagers is another prominent application of this material.[6,7] Furthermore, the application of amorphous silicon layers in highly textured solar cells to improve their conversion efficiency has drawn significant attention.[1,8,9]

Moreover, amorphous silicon is a promising material in the field of Li-ion batteries. Graphite is the common anode material in commercial Li-ion batteries. However, its specific capacity is only 372 mAh/g, which is a modest value. So it cannot meet the demands of higher energy density for future portable electronics, electric and hybrid vehicles, and renewable energy applications. Intensive research is currently ongoing to identify higher capacity anode materials for the next generation of lightweight and compact Li-ion batteries.[10] An attractive candidate to replace carbonaceous anodes is silicon, which has the highest theoretical specific capacity, in excess of 4000 $mAhg^{-1}$ and low discharge voltage upon intercalation of 4.4 Li atoms per Si atoms.[11] However, the Li incorporation into silicon involves almost a three-fold increase in its specific volume, leading to disintegration of crystalline Si electrodes. Thus, its capacity fades away if cycling is quite rapid. Although both amorphous and crystalline Si have a similar specific capacity to store Li^+, upon lithium insertion, amorphous Si does not disintegrate as intensely as its crystalline counterpart. Studies have shown that homogenous volume expansion in amorphous Si causes less pulverization and better cycling performance.[10] To overcome the above issue, nanostructuring of silicon film has been considered as a suitable approach.[12]

In this paper, we report the formation of high aspect-ratio amorphous silicon nanostructures using hydrogen-assisted deep reactive ion etching (H-DRIE) as a top-down process compatible with large area applications. Since the processing is achieved on amorphous silicon layers, it can be performed on SiO_2/Si as well as on glass substrates. Moreover, the use of flexible substrates such as stainless steel is conceivable. Apart from standard lithography, we have used our recently reported nanosphere colloidal lithography method to fabricate amorphous silicon vertical nanorods on SiO_2 underlayers.[13] As an immediate application of such highly featured structures, we have examined the performance of vertically etched a-Si nanorods as Li-ion batteries electrodes. The galvanostatic charge-discharge tests were performed on such arrays of amorphous silicon nanorods to demonstrate their suitability for high current level Li-ion battery applications.

The a-Si:H films were deposited in a radio frequency plasma enhanced chemical vapor deposition (RF-PECVD) unit operated at 13.56 MHz. The deposition temperature, pressure, and power density were set at 300 °C, 2 Torr, and 0.3 W/cm^2, respectively. A mixture of SiH_4 and H_2 was used as the source gas during the deposition. After deposition of amorphous silicon, the samples were coated with a layer of Cr with a thickness of 10 nm and patterned to act as the hard mask in the DRIE process for etching into desired a-Si:H structures. Figure 1(a) shows scanning electron microscopy (SEM) image of a 10 μm thick a-Si:H film deposited on glass. Raman spectroscopy of the sample shows the typical broad peak around 480 cm^{-1} corresponding to amorphous Si layer (inset of Fig. 1(a)). The evolution of vertical features of the amorphous silicon film is based on deep reactive ion etching of silicon for which a programmable mixture of oxygen, hydrogen, and SF_6 is used in an RIE unit with 13.56 MHz source. The deep etching consists of two consecutive steps; etching and passivation. During the etching step, only SF_6 is fed into the reactor for a short period of time (9–17 s), and the plasma power is set at 170 W. The

[a)]Author to whom correspondence should be addressed. Electronic mail: mohajer@ut.ac.ir

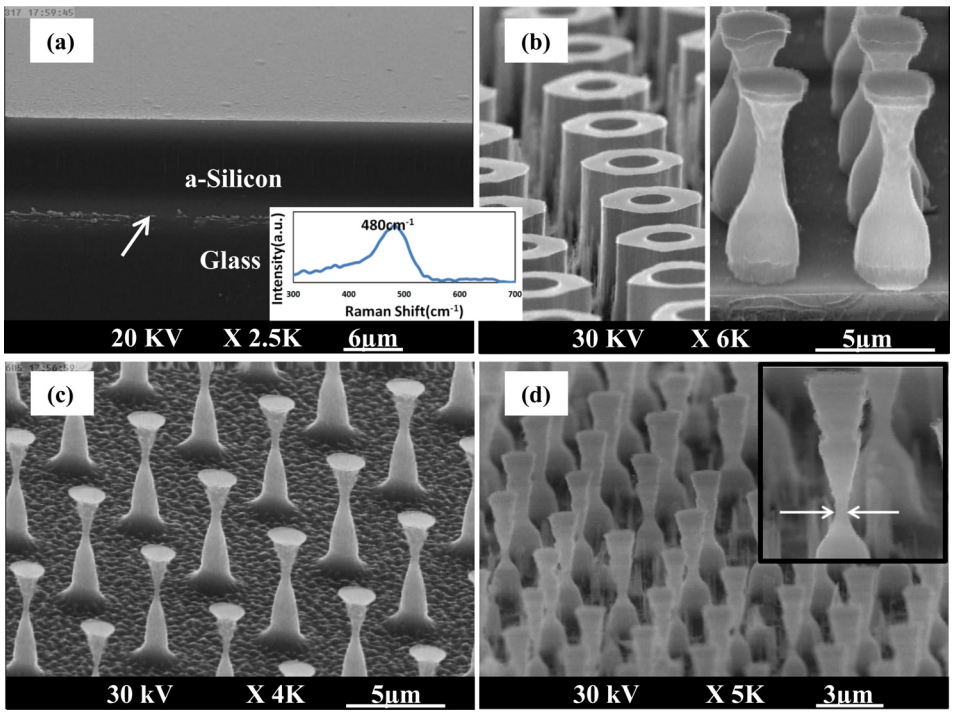

FIG. 1. SEM image of (a) 10 μm-thick a-Si:H film deposited on glass, indicating a smooth surface. Arrow points at the glass-film interface. Inset shows the Raman spectrum of the deposited Si film. (b)–(d) show the evolution of highly featured structures to demonstrate the ability of this deep etching technique in controlling the profile of each feature independently. The neck diameter in (d) is around 200 nm.

passivation step is critical for the formation of either vertical or three-dimensional structures. For vertical features, hydrogen, oxygen, and SF_6 are flown into the reactor with duration of 50 s and a plasma power of 170 W. If under-etching is desired (as in the three-dimensional features), the duration of the passivation sub-cycle is set at 30 s, and the plasma power is maintained at a lower value of 125 W.

Apart from vertical etching, one can program the procedure to arrive at highly featured three-dimensional structures at both micro and nano scales. In Figure 1(b), two arrays of hollow structures and curved features are placed aside. In parts (c) and (d), more complex features are demonstrated. The features of such complex structures can be controlled by properly adjusting the etching and the passivation sub-sequences.

Figure 2 collects the results of high aspect ratio amorphous silicon rods formed using a combination of nanosphere lithography and high-precision deep etching. Polystyrene nanospheres with diameters of 300 and 460 nm were self-assembled onto the surface by spin-coating (Fig. 2(a)). Then, a thin nickel layer was electron-beam evaporated to act as a hard-mask for subsequent etching purposes. After lifting-off the 300 nm polystyrene beads through sonication in dichloromethane solution for 4 min, 50–60 nm triangular nickel masks in hexagonal pattern were produced (inset of

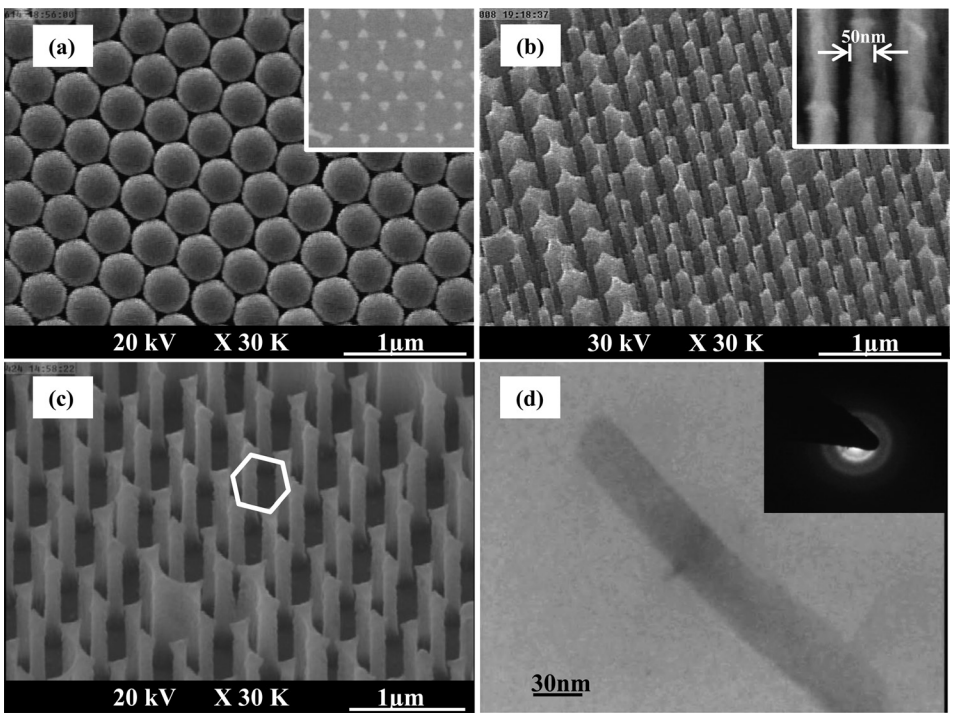

FIG. 2. (a) Primary nanospheres placed in an array format. Inset shows the evolution of ultra-small features of nickel after PS lift-off. (b) and (c) tilted views of highly ordered hexagonal vertical features of amorphous silicon nanorods formed by nanosphere lithography and vertical etching in RIE. Inset of (b) shows the formation of well-resolved nanorods with the width of 50 nm. (d) Transmission electron microscopy image plus diffraction pattern of an a-Si nanorod.

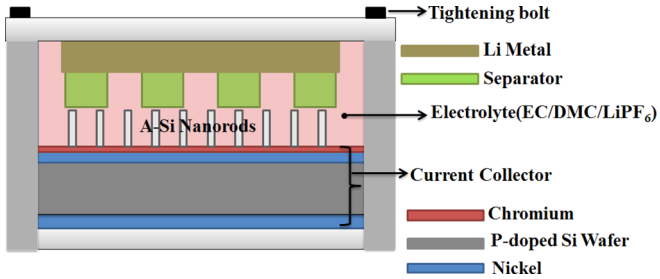

FIG. 3. Schematic representation of the fabricated lithium ion battery based on a vertically aligned a-Si nanorod array.

Fig. 2(a)). Next, the samples were vertically etched using RIE technique. Tilted views of highly ordered hexagonal vertical features of amorphous silicon nano-pillars are given in parts (b) and (c) of Figure 2. The inset in part (b) depicts the formation of nanorods with the width of 50 nm. Finally, the transmission electron microscopy (TEM) image of a fabricated a-Si:H nanorod in part (d) shows the amorphous nature of the nanorods after the process completion, which is also corroborated by the electron diffraction pattern in the inset of this image.

As mentioned above, we examined the efficiency of the fabricated a-Si nanorod arrays as a Li-ion battery electrode. Figure 3 shows a schematic view of the assembled battery. We employed Li metal as the counter electrode. The electrolyte in this battery consisted of 1M $LiPF_6$ in ethylene carbonate (EC)/dimethyl carbonate (DMC) (1:1 wt) solution. Also, polypropylene film was used as the separator.

To provide proper ohmic contacts to the silicon wafer, we used a p-doped silicon wafer coated with 70 nm Ni on its back and front sides. The front side of the silicon wafer has been further coated with a 20 nm chromium layer just on the previously coated nickel film to improve the adhesion of a-Si:H film and to provide appropriate ohmic contact. Moreover, the deposited layers serve as barriers against the lithium ion diffusion into the silicon wafer. Next, vertical nanorods with 750 nm height were fabricated as outlined previously. Finally, the charge-discharge rate performance of the nanorods versus Li/Li^+ electrode was evaluated using galvanostatic tests. For comparison, similar tests were performed on a planar a-Si:H film with a thickness of 750 nm. Figure 4(a) shows the voltage versus charge state profiles for the first and second cycles of the nanorod array cycled at a high rate of 1.2C. A so-called "C"-rate is a measure of the rate at which a battery is discharged (or charged) relative to its theoretical capacity. In general, "1C" rate corresponds to a current at which the battery will be discharged (charged) theoretically in 1 h.[14] The obtained profiles (Fig. 4(a)) show a sharp drop with a long flat plateau during the first discharge period where a-Si alloys with Li to form amorphous Li_xSi. These results are in general agreement with previous reports.[15,16] The first cycle discharge specific capacity was 3914 mAh/g, which is slightly lower than the theoretical specific capacity of silicon (4200 mAh/g). This could be caused by the extended polarization effects due to high discharge rate, although other parameters as working temperature might be responsible, too.[16]

By referring to Figures 4(a) and 4(b), the first charge specific capacity was 2348 mAh/g giving the first cycle a coulombic efficiency of 60%. Coulombic efficiency is a measure of the fraction of the lithium ions stored in the sample during a subcycle that are recoverable during the subsequent subcycle. Here, coulombic efficiency of a cycle is calculated through dividing the value of charge capacity by the value of discharge capacity. This irreversible capacity loss during the first cycle could be attributed to Solid Electrolyte Interphase (SEI) formation at the anode.[17] The second discharge specific capacity decreased to 3691 mAh/g; however, the second charge specific capacity increased to 2401 mAh/g indicating the columbic efficiency of 65%. As Figure 4(b) reveals, after the second cycle, the discharge capacity abruptly diminished by 21% (but not the charge capacity) giving the third cycle the discharge specific capacity of 2923 mAh/g. Afterwards, the capacity fading rate significantly decreased; so that the average discharge and charge capacity fading rates of cycles 3 to 25 were 4.6% and 2.9%, respectively. Even after 25 cycles of charge and discharge with such a high rate (1.2C), the sample discharge and charge capacities were 1244 mAh/g and 1156 mAh/g, considerably higher than graphite anodes

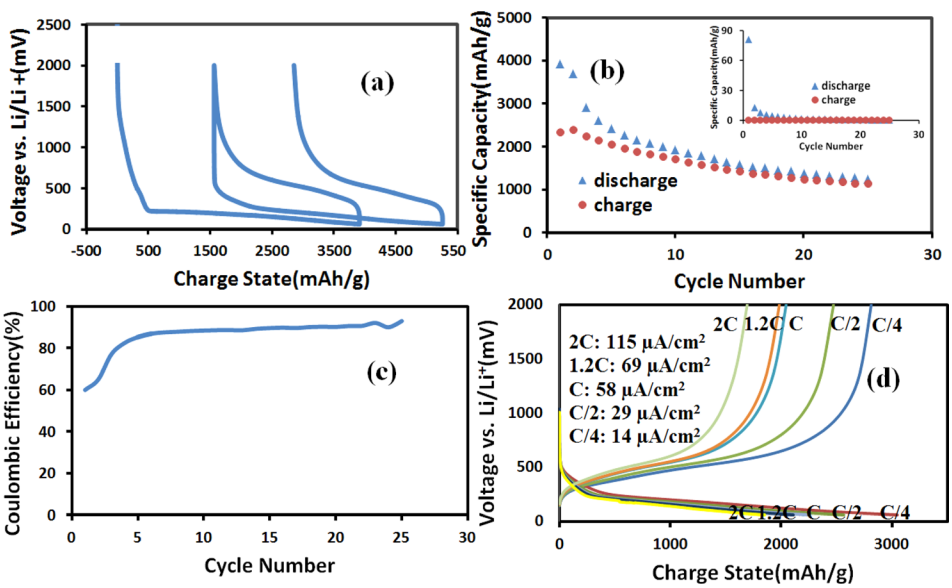

FIG. 4. Galvanostatic characteristics of a-Si:H nanorod arrays: (a) voltage vs. charge state profiles for the first and second galvanostatic cycles at 1.2C rate. (b) The specific capacity vs. cycle number at 1.2C rate showing the discharge (triangles) and charge (circles) specific capacities. Inset shows the same profile for a-Si planar film. (c) The coulombic efficiency vs. cycle number cycled at 1.2C rate. (d) The voltage vs. charge state profiles at five different C-rates. The inserted legend shows equivalent current density values corresponding to each rate.

with a theoretical specific capacity of 372 mAh/g.[18] Moreover, during the cycling process, coulombic efficiency increased to finally reach a high value of 93% after 25 cycles (Fig. 4(c)). It is worth noting that the rate at which this galvanostatic test was performed (1.2C) is considered a high rate, while the capacity of a battery usually decreases with increasing the test current due to amplified polarization effects. This statement is confirmed experimentally in Figure 4(d), which shows charge and discharge curves of the nanostructured sample at various rates. This figure demonstrates that the sample capacity is higher at lower rates.

The same galvanostatic charge-discharge tests (with 1.2C rate) were also performed on an a-Si:H planar film. We have observed that amorphous silicon planar film cannot be cycled efficiently at such a high rate (inset of Fig. 4(b)). SEM analysis of this sample after the galvanostatic test showed that the weak performance of the sample is due to the formation of a thick passivation layer on the sample during the first discharge, after which Li ions cannot effectively reach the a-Si surface.[14] After this step, the cell will mainly be charged and discharged capacitively rather than by a faradic mechanism where the electrodes act like the planes of a simple capacitor with an insulator between them.[19]

One main reason behind the observed high performance of amorphous silicon nanorods as opposed to planar a-Si film could be their significantly larger active surface area causing their corresponding current density to be markedly lower than that of an a-Si:H planar film. Hence, the damage inflicted on a-Si:H nanorods upon cycling at high rates will be less. The approximate surface area enhancement (A) for the nanostructured sample (a-Si:H nanorods with hexagonal pattern) was estimated as:

$$A = 14.5\frac{rh}{s^2},$$

where "r" and "h" denote the average radius and height of rods, and "s" represents the spacing between the initial polystyrene nanospheres measured between their centers. In our experiment, these values were r:50 nm, s:460 nm, and h:750 nm, yielding A:2.57. Thus, the effective current density was only 69 μA/cm^2 for the hexagonal patterned a-Si nanorod array with 1.2C = 100 μA, while this value was 1000 μA/cm^2 for the planar a-Si film with 1.2C = 560 μA. Another reason for the improved performance of the nanorod sample may be their ability to accommodate volume changes and the resulting strain without pulverization and the corresponding loss of contact.

In summary, we have fabricated highly featured amorphous silicon nanorods in large area by means of nanosphere lithography and hydrogen-assisted deep reactive ion etching. The ability of depositing thick and smooth films with good adhesion to the substrate allows one to realize high performance batteries with a-Si electrodes. Such devices are suitable for high-current applications, e.g., electric vehicle batteries.

The authors wish to thank Mr. A. Akhavan Farahani and Ms. F. Salehi for their technical support. The partial financial support of the University of Tehran was acknowledged.

[1]J. Zhu, Z. Yu, G. F. Burkhard, C. M. Hsu, S. T. Connor, Y. Xu, Q. Wang, M. McGehee, S. Fan, and Y. Cui, Nano Lett. **9**(1), 279–282 (2009).
[2]S. Murugesan, J. T. Harris, B. A. Korgel, and K. J. Stevenson, Chem. Mater. **24**(7), 1306–1315 (2012).
[3]K. H. Cherenack, A. Z. Kattamis, B. Hekmatshoar, J. C. Sturm, and S. Wagner, IEEE Electron Dev. Lett. **28**(11), 1004–1006 (2007).
[4]B. D. Yang, J. M. Oh, H. J. Kang, S. H. Ko Park, C. S. Hwang, M. K. Ryu, and J. E. Pi, ETRI J. **35**(4), 610–616 (2013).
[5]E. Lausecker, Y. Huang, T. Fromherz, J. C. Sturm, and S. Wagner, Appl. Phys. Lett. **96**(26), 263501 (2010).
[6]K. S. Karim, G. Sanaie-Fard, T. Ottaviani, M. H. Izadi, and F. Taghibakhsh, J. Korean Phys. Soc. **48**(91), S85–S91 (2006).
[7]F. Taghibakhsh, I. Khodami, and K. S. Karim, IEEE Trans. Electron Dev. **55**(1), 337–342 (2008).
[8]C. H. Yang, C. Y. Hsueh, D. J. Yeh, C. I. Ho, C. M. Leu, Y. H. Yeh, and S. C. Lee, IEEE Electron Device Lett. **32**(9), 1254–1256 (2011).
[9]W. C. Tu, Y. T. Chang, C. H. Yang, D. J. Yeh, C. I. Ho, C. Y. Hsueh, and S. C. Lee, Appl. Phys. Lett. **97**(19), 193109 (2010).
[10]H. Ghassemi, M. Au, N. Chen, P. Heiden, and R. Yassar, ACS Nano **5**(10), 7805–7811 (2011).
[11]B. Bang, M. Kim, H. Moon, Y. Lee, and J. Park, J. Power Sources **156**(2), 604–609 (2006).
[12]R. Teki, M. Datta, R. Krishnan, T. Parker, T. Lu, P. Kumta, and N. Koratkar, Small **5**(20), 2236–2242 (2009).
[13]M. Poudineh, Z. Sanaee, A. Gholizadeh, S. Soleimani, and S. Mohajerzadeh, IEEE Trans. Nanotechnol. **12**(5), 712–718 (2013).
[14]See supplementary material at http://dx.doi.org/10.1063/1.4902068 for describing the galvanostatic measurement of amorphous silicon of Li-ion batteries.
[15]C. K. Chan, H. Peng, G. Liu, K. McIlwrath, X. F. Zhang, R. A. Huggins, and Y. Cui, Nat. Nanotechnol. **3**(1), 31–35 (2008).
[16]U. Kasavajjula, C. Wang, and A. J. Appleby, J. Power Sources **163**(2), 1003–1039 (2007).
[17]S. P. V. Nadimpalli, V. A. Sethuraman, S. Dalavi, B. Lucht, M. J. Chon, V. B. Shenoy, and P. R. Guduru, J. Power Sources **215**, 145–151 (2012).
[18]K. Karki, Y. Zhu, Y. Liu, C. F. Sun, L. Hu, Y. Wang, C. Wang, and J. Cumings, ACS Nano **7**(9), 8295–8302 (2013).
[19]J. Vetter, P. Novak, M. R. Wagner, C. Veit, K. M. Moller, J. O. Besenhard, M. Winter, M. Wohlfahrt-Mehrens, C. Vogler, and A. Hammouche, J. Power Sources **147**(1), 269–281 (2005).